BBA - Molecular Cell Research 1873 (2026) 120110

Contents lists available at ScienceDirect

BBA - Molecular Cell Research

journal homepage: www.elsevier.com/locate/bbamcr

Research Paper

ATM kinase phosphorylates HSP90 on T297 changing its conformation dynamics and promoting its interaction with HER2 receptor tyrosine kinase

Giulia Fianco [a,b,1], Irene Taddei [b,c,d,1], Veronica Oropallo [b,c,d], Claudia Contadini [c,e], Alessandra Ferri [b,c,d,f], Laura Coculo [a,b], Stefano A. Serapian [g], Giorgio Colombo [g], Venturina Stagni [a,b,*,2], Daniela Barilà [b,c,*,2]

[a] Institute of Molecular Biology and Pathology, National Research Council (CNR), 00185, Rome, Italy
[b] Laboratory of Cell Signaling, IRCCS-Fondazione Santa Lucia, 00179, Rome, Italy
[c] Department of Biology, University of Rome "Tor Vergata", 00133, Rome, Italy
[d] PhD program in Cellular and Molecular Biology, Department of Biology, University of Rome "Tor Vergata", 00133, Rome, Italy
[e] Preclinical Models and New Therapeutic Agents Unit, IRCCS Regina Elena National Cancer Institute, 00144, Rome, Italy
[f] Department of Pathology and Laboratory Medicine, Meyer Cancer Center, Weill Cornell Medical Center, New York, NY, USA
[g] Department of Chemistry, University of Pavia, v.le Taramelli 12, 27100, Pavia, Italy

ARTICLE INFO

Keywords:
ATM kinase
HSP90 chaperone
Breast Cancer
HER2 receptor

ABSTRACT

Heat Shock Protein 90 (HSP90) is an essential molecular chaperone whose activity is regulated not only by co-chaperones but also by distinct post-translational modifications. Interestingly, its chaperone activity is essential for the stability of several oncogenes, among which the receptor tyrosine kinase HER2. HER2 is overexpressed in 20–30% of breast and ovarian cancers. Its overexpression triggers proliferative and transforming pathways aberrant activation and therefore frequently correlates with invasive and poor prognostic features, and associates with shorter patient survival. Of note, HSP90 inhibitors have been studied in HER2-positive breast cancer and have shown promising results. Unexpectedly, we previously reported that ATM promotes the interaction of HER2 with HSP90 therefore sustaining HER2 protein stability and tumorigenicity.

To further investigate the interplay between HER2-HSP90 and ATM, we tested the hypothesis that ATM could phosphorylate HSP90. We confirmed that ATM activation can induce the phosphorylation of HSP90 in HER2 positive breast cancer models. Point mutagenesis showed that T297 is the major site targeted by ATM kinase and importantly the unphosphorylatable mutant HSP90-T297A displays a reduced ability to interact with HER2, and to prevent its ubiquitination and degradation. Consistently, the overexpression of HSP90-T297A impinges on the viability of HER2-overexpressing cells, further supporting a role of this phosphorylation in the modulation of HER2 tumorigenicity. T297 is located in the middle domain of HSP90, a region that is involved in the interaction of HSP90 with clients. Consistently, structural studies indicate that T297 phosphorylation can indeed favor the chaperone's interaction with HER2, further supporting our hypothesis.

1. Introduction

The 90 kDa Heat Shock Protein (HSP90) is a chaperone protein essential for the maintenance of cellular homeostasis [1] and its function ensures the cellular physiological processes controlling protein quality and stability. HSP90 is a dimeric protein very abundant in eukaryotic cells and it can constitute up to 1–2% of the cellular proteins under normal conditions [2]. It is mostly localized in the cytosol, where two strongly homologous but functionally distinct isoforms have been identified: an inducible form (HSP90α) [3,4] and a constitutive form (HSP90β) [5]. A minor fraction is also reported to be in the nucleus and in cellular organelles [6].

Under physiological conditions, HSP90 works together with other Heat Shock Protein family members (HSPs) and co-chaperones forming the cellular assembly machine and promoting the formation of the correct conformation of more than 200 proteins, called HSP90 "clients"

* Co-last and co-corresponding.
E-mail addresses: venturina.stagni@cnr.it (V. Stagni), daniela.barila@uniroma2.it (D. Barilà).
[1] These authors contributed equally to this work.
[2] These authors contributed equally to this work.

https://doi.org/10.1016/j.bbamcr.2026.120110
Received 15 April 2025; Received in revised form 12 December 2025; Accepted 7 January 2026
Available online 9 January 2026

[2,7], ensuring their complete maturation, correct folding and stability. At the same time, HSP90 stabilizes the exposed catalytic domains of some protein kinases, sustaining their activity [8]. Conversely, the dissociation of HSP90 machinery-clients interaction leads to the accumulation of unfolded HSP90 client proteins within the cell and to the recruitment of E3 ubiquitin ligases that target these proteins for degradation [9,10].

Tumor cells often show a dramatic increase of HSP90 expression compared to normal cells, suggesting its important role in this context in buffering cellular stresses induced by the malignant conditions [11]. Indeed, HSP90 expression and activity ensure the folding and stability of several oncoproteins, including many kinases and transcription factors, that are mutated, translocated, amplified, or overexpressed in malignancy *e.g.* HER2 transmembrane kinase, BCR-ABL kinase, AKT kinase, mutated p53 protein [11]. These findings revealed a fundamental role of HSP90 in the progress of malignant diseases.

Given its role in stabilizing proteins that aid cancer progression, the possibility of targeting HSP90 activity is a promising therapeutic strategy for cancer treatment [11,12]. In particular, since it is well known that HSP90 is an ATPase chaperone protein and its functionality is strictly dependent on the binding and hydrolysis of ATP [13], several molecules that specifically inhibit HSP90 by blocking ATP access to the ATP binding pocket have been generated and are to date in clinical trial reviewed in [14]. In parallel, efforts have been devoted to the development of allosteric modulators of HSP90 [15–17] as well as to disruptors of HSP90 client and co-chaperone interactions [18]. These molecules perturb the HSP90 chaperone machine preventing its association to its client proteins including those responsible for tumor progression which are therefore directed to degradation [19,20].

HER2 receptor tyrosine kinase is an HSP90 client oncoprotein and the chaperone system controls the stability of both nascent and mature protein, finely modulating its expression and activity [20]. HER2 is overexpressed in 20–30% of breast and ovarian cancers and its gene is also amplified in other common types of cancers including lung, gastric, and oral cancers [21]. Its overexpression triggers proliferative and transforming pathways aberrant activation and thus frequently correlates with invasive and poor prognostic features and a shorter patient survival [22]. The prognosis of HER2 positive tumor patients improved significantly upon the development of molecular targeted approaches, such as Trastuzumab, a humanized monoclonal antibody targeting HER2 [23].

The regulation of HSP90 functionality by using molecules that block ATP binding to HSP90 is reported to be an efficient way to enhance HER2 degradation, resulting in polyubiquitination and subsequent downregulation of its expression levels [24].

In recent years, an additional layer of regulation of HSP90 function has been reported. Many groups demonstrated that HSP90 functionality is tightly controlled by several post-translational modifications (PTMs), especially by phosphorylation [25,26]. Indeed, they reported HSP90 phosphorylation by several protein kinases on specific phosphosites, including casein kinase II [27], DNA-dependent protein Kinase and Wee1/Swe1 kinase [28], and they demonstrated that changes in its phosphorylation status have a deep impact on the chaperone functionality [29,30].

ATM is a serine/threonine protein kinase, whose expression is lost in a rare autosomal genetic disorder named Ataxia Telangiectasia (A-T), that phosphorylates its substrates on specific serine/threonine residues preferentially followed by a glutamine residue, called S/T-Q motifs, following its activation [31]. ATM is historically considered a central player of the DNA damage response (DDR) and its double-stranded breaks (DSBs) mediated activation triggers the downstream phosphorylation and modulation of several target proteins [32], in order to prevent genomic instability [33]. In recent years, growing evidences brought to light several additional functions of ATM kinase, not limited to the DDR in the nucleus of the cell, including a role in response to oxidative stresses and in autophagy mechanism (reviewed in [34–36]). Moreover, proteomic analyses have identified over 700 putative ATM substrates, further supporting its involvement in multiple novel cellular pathways [37,38].

We previously reported a non-canonical role of ATM kinase as promoter of HER2 tumorigenicity in breast cancer [39]. We described a positive feedback loop in which HER2 triggers ATM kinase activity and, conversely, ATM is essential for HER2 protein stability ensuring its association with HSP90 that represents the principal modulator of its folding and stability. Pharmacological or genetic inhibition of ATM activity or expression results in the release of HER2 from HSP90 which in turn promotes HER2 ubiquitination and degradation [39].

Here we show that HER2 overexpression triggers ATM-dependent HSP90 phosphorylation *in vitro* and *in vivo*. We also provide evidence for ATM-dependent phosphorylation of HSP90β on T297 residue. Structural analysis and comparative Molecular Dynamics (MD) simulations of *wild-type* HSP90β and its T297-phosphorylated variant indicate that the PTM impacts on the internal dynamics of the chaperone, increasing structural rigidity in the phosphorylated form and pre-organizing the client binding site in a favorable dynamic state to lock HER2 once recruited. In addition, we provide evidence for the ability of the ATM dependent phosphorylation of HSP90 on T297 as a novel mechanism to promote HSP90 chaperone functionality, sustaining HER2 protein levels, stability and *in vitro* tumorigenicity.

2. Results

2.1. ATM kinase promotes HSP90 phosphorylation on T297 in HER2 positive breast cancer models

We have previously shown that ATM kinase promotes the ability of HSP90 to interact and stabilize HER2 [39].

To get more insights into the molecular mechanism, we tested the hypothesis that ATM could drive HSP90 phosphorylation. To this aim, HSP90 was immunoprecipitated from protein extracts derived from the human HER2 positive cell line SKBR3, and its phosphorylation revealed using a phospho-S/T-Q antibody that selectively recognize proteins phosphorylated in the consensus motif for ATM/ATR kinases [31,40]. More interestingly, the pretreatment with ATM kinase inhibitor KU-55933, as expected, prevented ATM auto-phosphorylation on S1981 and more importantly partially impinged on HSP90 phosphorylation (Fig. 1A).

To further strength this result, we adopted a transgenic mouse model expressing rat HER2/NeuT oncogene in the mammary gland. These mice develop HER2 positive mammary tumors spontaneously 15 weeks after birth. Using this system, we have previously shown that ATM is active and phosphorylated on S1981 in these tumors [39]. The *in vivo* administration of KU-55933 by intraperitoneal injection downregulates ATM phosphorylation on S1981 and, most importantly, decreases HER2 expression [39]. HSP90 was immunoprecipitated from tumors derived from HER2/NeuT mice pretreated or not with the ATM kinase inhibitor KU-55933 (Fig. 1B). For each condition, four tumors were pooled together (Supplementary Fig. S1A). Immunoblotting analysis with a phospho-S/T-Q antibody confirmed that HSP90 is phosphorylated on S-/T-Q *in vivo* and its phosphorylation is strongly affected by the inhibition of ATM kinase activity (Fig. 1B).

HSP90β is reported as a constitutively expressed protein and generally more abundant compared to the inducible HSP90α isoform in several cell lines (reviewed in [3]). We, therefore, focused our attention on HSP90β isoform. To further evaluate the ability of ATM kinase to phosphorylate HSP90β, we immunoprecipitated ATM from HEK293T cells and assayed its ability to phosphorylate a human recombinant purified HSP90β *in vitro*. Immunoblotting with anti-pS/T-Q antibody confirmed this phosphorylation (Fig. 1C).

The ability of ATM to phosphorylate HSP90β was also confirmed by transient transfection experiments in HEK293T cells. We transiently overexpressed HA-HSP90β isoform in HEK293T cells and ATM kinase

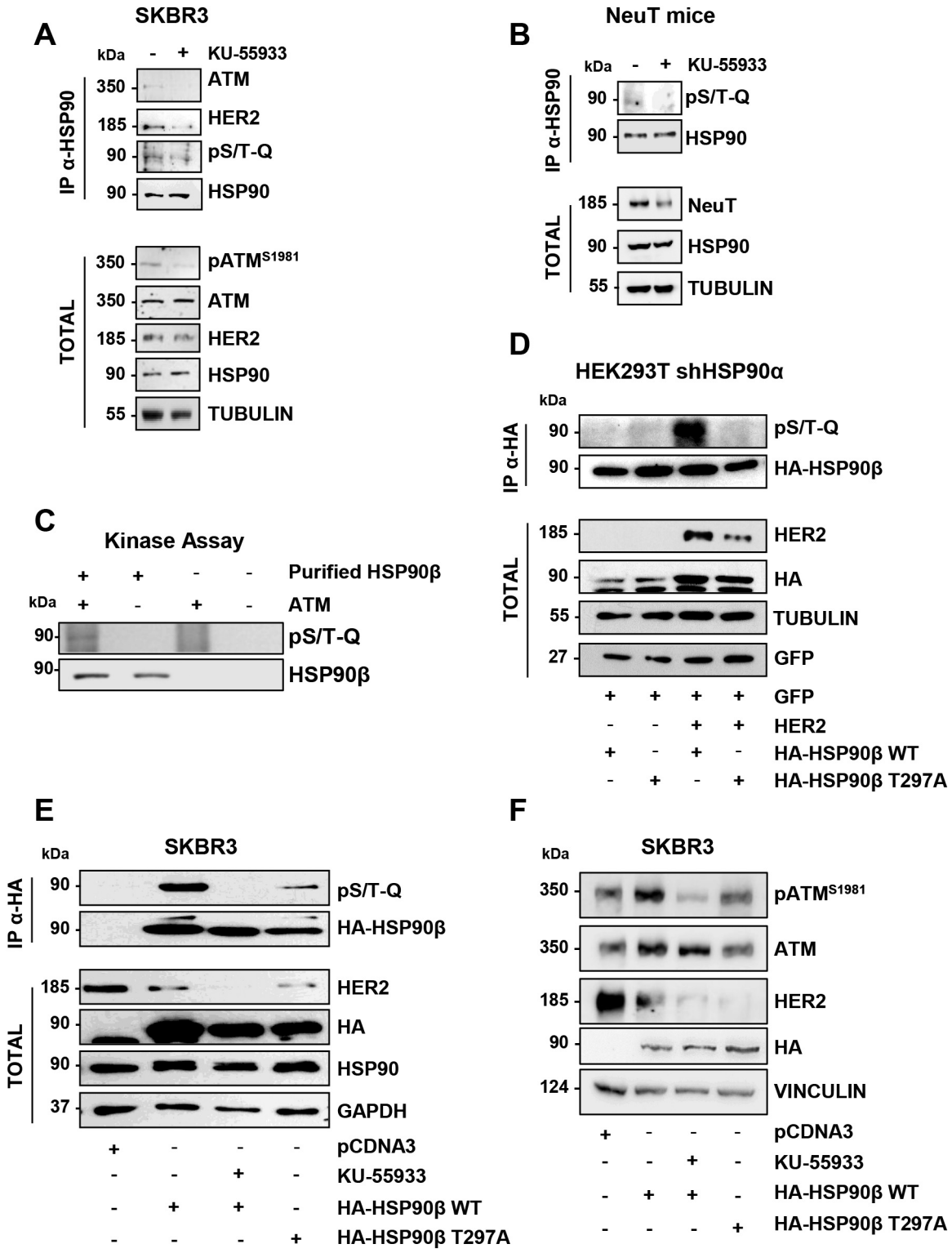

Fig. 1. HER2 promotes ATM-dependent phosphorylation of HSP90. (A) Representative Western blot showing immunoprecipitation of endogenous HSP90 on SKBR3 (HER2+++) cells treated or not with KU-55933 (10 μM, 12 h) as indicated. (B) Representative Western blot showing immunoprecipitation of endogenous HSP90 from protein extracts derived from mouse mammary tissue ($n = 4$). FBV-NeuT mice were intraperitoneally injected with 10 mg kg^{-1} KU-55933 in DMSO or with DMSO as control, every 2 days for 2 weeks starting from the appearance of the first mammary tumor, and sacrificed 3 days after the last injection [39]. (C) Representative Western blot showing kinase assay performed using immunoprecipitated human ATM from HEK293T cells and recombinant purified human HSP90β. (D) Representative Western blot showing immunoprecipitation of HA-HSP90β from protein extract of HEK293T cells transfected as indicated. GFP construct was used as control of transfection. (E) Representative Western blot showing immunoprecipitation of HA-HSP90β from protein extract of SKBR3 (HER2+++) cells transfected as indicated and treated or not with KU-55933 (10 μM, 12 h). (F) Representative Western blot showing $pATM^{S1981}$, ATM and HER2 protein levels in SKBR3 (HER2+++) cells transfected as indicated and treated or not with KU-55933 (10 μM, 12 h).

activity was triggered either by its overexpression alone [41], or by overexpression followed by DNA damage induction using the radiomimetic drug Neocarzinostatin (NCS), or alternatively by HER2 overexpression [39] (Supplementary Fig. S1B). HSP90β was selectively immunoprecipitated and its phosphorylation was revealed by immunoblotting. Importantly, we could show that HSP90β isoform is phosphorylated on S/T-Q residues following ATM activation in all three conditions (Supplementary Fig. S1B).

The analysis of HSP90β isoform protein sequence revealed the presence of two Serine (S206 and S460) and two Threonine (T297 and T479) residues as potential ATM target sites because located in the S/T-Q motifs [31]. Interestingly, HSP90β phosphorylation on T297 has been

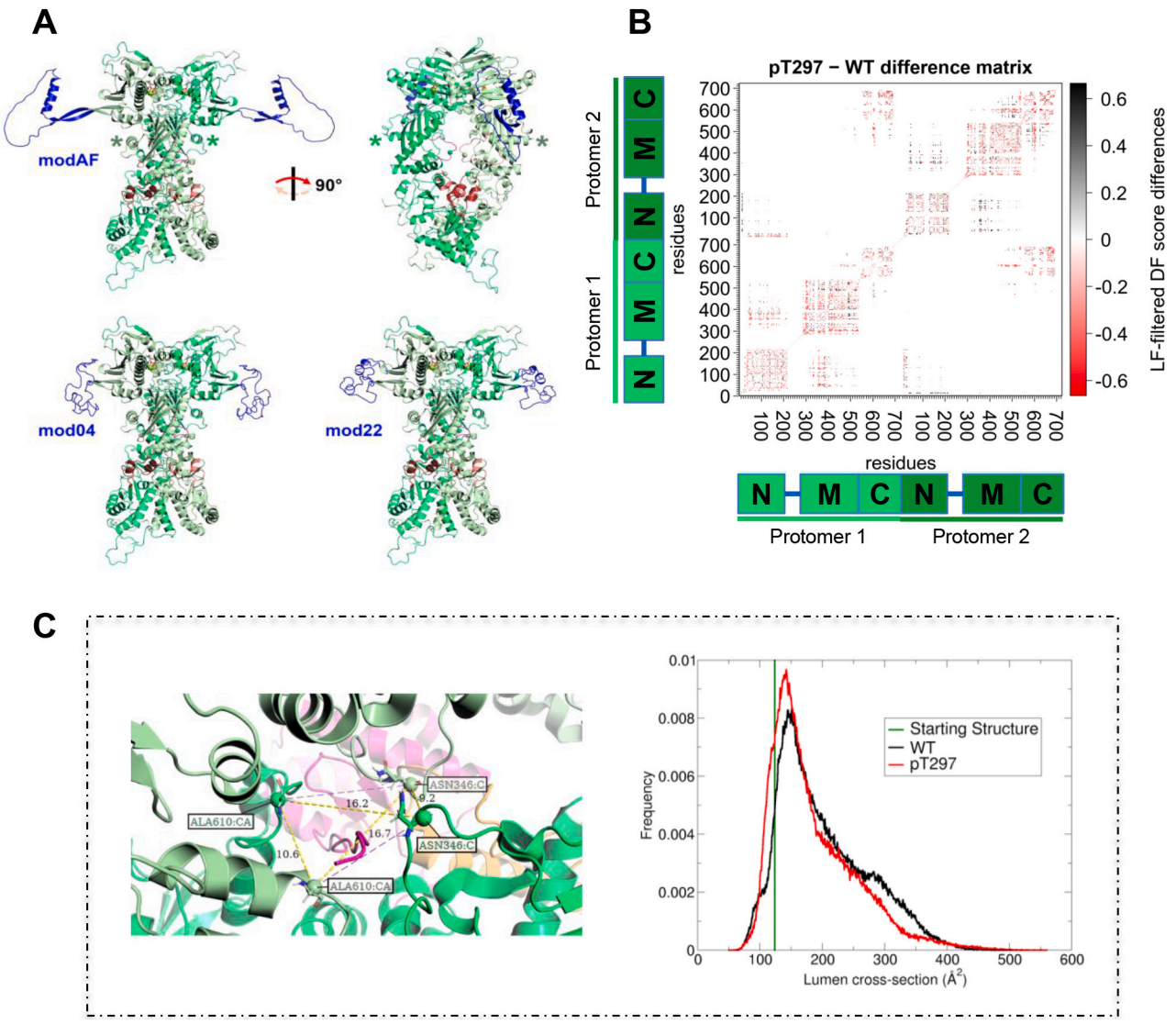

Fig. 2. HSP90β phosphorylation on T297 modifies the chaperone's functional dynamics and recognition mechanisms. (A) Overview of phosphorylation site T297 and of the three HSP90β charged loop models developed for the MD simulations run in this work (more details in the main text); identical copies of each model are incorporated into protomer A and protomer B of our loopless starting structure and are shown in blue. Structures on the bottom bear two copies of loop models mod04 and mod22, which were generated by the MODELLER package [43]. The structure on the top left, with two copies of model modAF, originates from the AlphaFold database [44]; on the top right, it has been rotated counterclockwise by 90° with respect to the plane of the page, looking from the top. This is to reveal the location of the client binding lumen, delimited by the loops shown in red (also shown in the other structures for reference). Green spheres marked in the lumen represent carbon atoms used to quantify the lumen cross-section during simulations. Asterisks in the top two panels mark the T297 phosphorylation site on protomer A (duller green) and protomer B (brighter green; heavy atoms rendered as sticks). ATP heavy atoms and Mg^{2+} are also rendered in each structure as sticks and a green sphere, respectively. The remainder of protomers A and B in each structure are also shown in duller and brighter shades of green, respectively. (B) Difference matrix of distance fluctuation (DF) scores, filtered by the Local Fluctuation (LF) value (see Materials and methods for formulae and details). Red areas show residue pairs undergoing a decrease in DF score upon phosphorylation (*i.e.*, increase in allosteric coordination); black areas denote areas where allosteric dialogue is lost upon phosphorylation. For reference, residues composing the N-terminal, Middle, and C-terminal domains of each HSP90β protomer are marked on the bottom axis. The charged loop is shown in blue. (C) HSP90β lumen and lumen cross-section. Right panel: Illustration of the HSP90β client-binding lumen as it appears in the HSP90β-CDC37-Cdk4 complex (PDB ID: 5fwk) [49], closely related to our starting structure. HSP90β protomers are rendered in the same shades of green as *2A*; cochaperone CDC37 is rendered in yellow; and client Cdk4—part of which is bound to the lumen as is the case with HER2—is rendered in magenta. Cα atoms in Ala610 and C atoms in Asn346, which are used as starting points to build the lumen cross-section in each frame, are rendered as spheres; the rest of the residues are rendered as sticks. Lines connecting spheres are to guide the eye; the real best-fit plane used to calculate the cross-section is not shown. Left panel: histogram comparing the distribution of lumen cross-sections in combined MD Simulations of WT_{AF}, WT_{04}, and WT_{22} (black) *vs.* combined MD simulations of $pT297_{AF}$, $pT297_{04}$, and $pT297_{22}$ (red). The cross-section in the starting structure is also shown, for reference (green line). (For interpretation of the references to color in this figure legend, the reader is referred to the web version of this article.)

previously identified in a wide phosphoproteomic study carried out in HEK293T cells treated with ionizing radiation to induce DNA damage and ATM kinase activation [37]. Importantly, sequence alignment analysis revealed that this residue is highly conserved throughout evolution (Supplementary Fig. S1C), supporting the idea that the T297 residue may play a functional role. To test whether T297 may indeed be the main target of ATM-dependent phosphorylation upon HER2 overexpression, we generated the HA-HSP90β T297A unphosphorylatable mutant. Previous work reported a role of ATM also in the phosphorylation of HSP90α isoform [42], therefore, to detect the HSP90β isoform-specific phosphorylation, we took advantage of HEK293T shHSP90α cells, stably silenced for HSP90α expression (Supplementary Fig. S1D). Cells were transiently transfected with HER2 and either HA-HSP90β WT or HA-HSP90β T297A. HA-HSP90β WT or HA-HSP90β T297A mutants were immunoprecipitated with anti-HA antibody and their phosphorylation was revealed by phospho-S/T-Q. Interestingly, HER2 overexpression triggered HA-HSP90β WT phosphorylation but failed to phosphorylate HA-HSP90β T297A, thereby driving the conclusion that T297 represented the main phosphorylation target (Fig. 1D). The same result was also obtained in SKBR3 cells that overexpress endogenous HER2. Again, the phosphorylation of the HA-HSP90β T297A mutant is severely impaired compared to what detected for HA-HSP90β WT and upon ATM kinase inhibition in the presence of KU-55933 (Fig. 1E). Remarkably, we observe a strong downregulation of HER2 levels and a slight reduction of ATM activity in the presence of HA-HSP90β T297A (Fig. 1F), suggesting that the effect of HA-HSP90β T297A on ATM activity is not very strong and could not account for the reduction of pS/T-Q signal.

2.2. *HSP90β phosphorylation on T297 modifies the chaperone's functional dynamics and recognition mechanisms*

To gain insight into how phosphorylation impacts on the molecular determinants underlying the functions of HSP90β, we set out to analyze and compare fully solvated atomistic Molecular Dynamics (MD) simulations of models of the protein in its WT and phosphorylated forms (henceforth pT297). Starting from a refined CryoEM structure of human HSP90β provided by the Agard lab, we additionally modeled the long unstructured loop present on each HSP90β protomer using both the MODELLER suite of programs [43] and the AlphaFold database (AF) [44]. We selected three loop models (2 from MODELLER runs, **mod04** and **mod22**, 1 from the AF database, **modAF**), as shown in Fig. 2A and discussed further below (see Materials and methods for details on the set up of the systems). Starting from these models, we modeled phosphorylation on T297 (Fig. 2A, asterisks indicating the phosphorylation location; see also Materials and methods) generating three additional different starting conformations for pT297-HSP90β.

Each of the six generated models for WT and pT297-HSP90β (3 + 3) was used to start 4 independent molecular dynamics (MD) simulations, for a combined total of 24 microseconds. Replicates for the three starting models of both variants (WT and pT297) were concatenated into two single metatrajectories, which could then be directly compared and analyzed.

Specifically, to quantify the effect of phosphorylation on T297 on the functionally oriented aspects of HSP90β dynamics, we calculated the coordination between distal residues, using Distance Fluctuation (DF) analysis. DF analysis reports on the coordination patterns in dynamics between any two residues of the protein, as a function of their pair-distance fluctuation. We previously showed that small DF values define (groups of) coordinated residues, which move in a cooperative manner determining the onset of functional motions [45–47]. Importantly, DF profiles may change in the presence/absence of a PTM such as pT297, allowing them to link internal dynamics with measured biological effects. Additionally, differences in the DF patterns of the WT and phosphorylated versions of HSP90β can unveil the substructures whose dynamic changes respond to the covalent modification, even if distal.

Interestingly, the difference matrix between the phosphorylated and the WT versions (Fig. 2B) shows that the former is generally more rigid. Interestingly, the decrease in internal flexibility reverberates across each domain (*cf.* domain maps at the bottom of Fig. 2B). At the same time, off-diagonal blocks indicate that the phosphorylation also alters the allosteric coordination between the two NTDs, between the NTD and Middle-domain, and the NTD and CTDs within each protomer. In protomer B, a significant decrease in flexibility in the phosphorylated form is noticeable for the region between the Middle-small and C-Terminal Domains (*cf.* redder areas in Fig. 2B): importantly, this region contains the lumen, where the client binding site is located.

On this basis, we calculated the area of the cross section of the lumen (Fig. 2C, right panel) from the respective metatrajectories of the two variants (see Methods): interestingly, despite decreased flexibility, the distribution of the area of the lumen (Fig. 2C, left panel) does not appear to change significantly, compared to the area of the lumen for the CryoEM structure of HSP90 in complex with the unfolded kinase CDK4 and co-chaperone CDC37.

Overall, these data show that phosphorylation on T297 remodels the coordination within and between HSP90β domains decreasing internal flexibility and likely enhancing the structural and dynamic pre-organization of the substructure of the chaperone that is required for client recognition. The PTM shows a pervasive effect throughout the whole structure, modifying internal dynamics of HSP90β well beyond the localized substructure where T297 is located.

2.3. *HSP90β phosphorylation on T297 promotes HER2 protein stability*

Molecular dynamics simulations show that phosphorylation of HSP90β on T297 alters the internal flexibility of its domains, which could impact the chaperone's recognition mechanisms and suggest that it may affect its interaction with HER2. We have previously shown that ATM promotes HER2 interaction with HSP90 and that ATM genetic or pharmacological inactivation resulted in a strong induction of HER2 protein ubiquitination [39]. According to our findings, we speculated that ATM may promote the interaction between HSP90 and HER2 by phosphorylating HSP90β on T297. To clarify this issue SKBR3 cells were transiently transfected with HA-HSP90β WT or with of HA-HSP90β T297A mutants. HER2 was immunoprecipitated with a specific antibody and HSP90 co-immunoprecipitation evaluated by immunoblotting with anti-HA antibody. As expected HER2 could efficiently interact with HA-HSP90β WT but not with HA-HSP90β T297A. Importantly, ATM kinase inhibition impaired this interaction similarly to what observed upon HA-HSP90β T297A transient transfection or upon HSP90 enzymatic activity inhibition, further supporting the requirement for ATM kinase-dependent phosphorylation on T297 for this interaction (Fig. 3A).

To investigate whether ATM-dependent phosphorylation of HSP90β on T297 may therefore affect HER2 protein stability, SKBR3 cells were transiently transfected with either HA-HSP90β WT or HA-HSP90β T297A. Cells were treated with Cycloheximide for different times to block nascent translation and HER2 protein levels revealed by immunoblotting. Indeed, HA-HSP90β T297A expression reduced HER2 protein half-life compared to HA-HSP90β WT (Fig. 3B), supporting a role for T297 phosphorylation in promoting HSP90 ability to sustain HER2.

According to our findings, we speculated that ATM may prevent HER2 ubiquitination by phosphorylating HSP90β on T297. To clarify this issue HER2 was immunoprecipitated from SKBR3 cells transiently transfected with HA-HSP90β WT, HSP90β T297A or HSP90β T297D, a phosphomimetic mutant, and its ubiquitination revealed by immunoblotting with anti-ubiquitin antibody. As expected, HER2 was not ubiquitinated in the presence of HA-HSP90β WT. Similar results were detected in the presence of the HA-HSP90β T297D mutant. Conversely, the overexpression of the HA-HSP90β T297A mutant significantly correlated with a dramatic increase of HER2 ubiquitination, similarly to what observed upon treatment with the HSP90 chaperone inhibitor, 17AAG (Fig. 3C). Overall, these experiments, allow the conclusion that

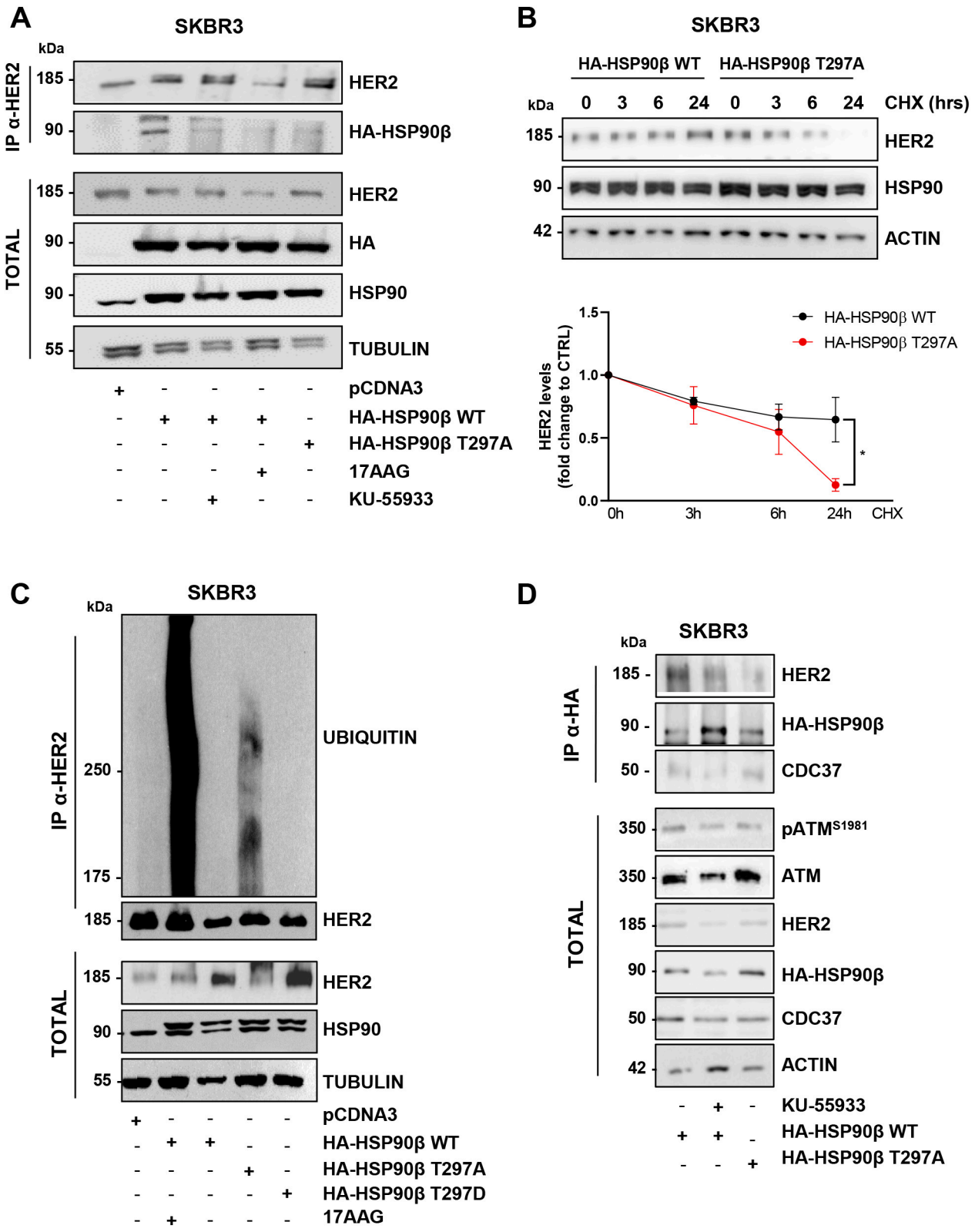

Fig. 3. HSP90β phosphorylation on T297 promotes HER2 protein stability and interaction. (A) Protein extracts from SKBR3 cell lines transfected as indicated and treated or not with 17AAG (1 μM, 4 h) or KU-55933 (10 μM, 12 h), were prepared for immunoprecipitation with anti-HER2 antibody and subjected to western blotting with anti-HSP90 antibody. (B) Cycloheximide (CHX) was used to inhibit protein synthesis in SKBR3 cells expressing HA-HSP90β WT and HA-HSP90β T297A. HER2 protein levels were evaluated in cell lysates by Western blotting. On the bottom, quantification of HER2 protein levels compared to the CTRL. To determine statistically significant differences, we performed unpaired *t*-Test between two group: *, $P \leq 0.05$ SKRBR3 HA-HSP90β T297A vs SKBR3 HA-HSP90β WT;(C) Protein extracts from SKBR3 cell lines transfected as indicated and treated or not with 17AAG (1 μM, 4 h) or KU-55933 (10 μM, 12 h), were prepared for immunoprecipitation with anti-HER2 antibody (normalizing on HER2 total protein) and subjected to western blotting with an anti-ubiquitin antibody. (D) Protein extracts from SKBR3 cell lines transfected as indicated and treated or not with KU-55933 (10 μM, 12 h), were prepared for immunoprecipitation with anti-HA antibody and subjected to western blotting with anti-CDC37 antibody.

ATM may significantly modulate HSP90β functionality *via* its phosphorylation on T297. Of note, co-chaperone CDC37 is required and important for the modulation of HSP90 kinase interaction [48] and HSP90-CDC37 complex synergistically acts as a facilitator of HER2 dependent oncogenesis [49]. Therefore, we can speculate that ATM-dependent phosphorylation of HSP90 may either directly affect its physical interaction with HER2, or alternatively impinge on HSP90-CDC37 interaction, and thus only indirectly impact on HSP90-HER2 binding. To clarify this issue, SKBR3 cells were transiently transfected with either HA-HSP90β WT or HA-HSP90β T297A and HSP90β immunoprecipitated with anti-HA antibody. Accordingly to Fig. 3A, HER2 co-immunoprecipitated with HA-HSP90β WT, but not with HA-HSP90β T297A or after treatment with KU55933 (Fig. 3D). Of note, when we probed the same samples for CDC37 co-immunoprecipitation using specific anti-CDC37 antibody, we revealed that CDC37 associated similarly with both HA-HSP90β WT and HA-HSP90β T297A. These results indicate that ATM-dependent phosphorylation on T297 does not affect the HSP90β-CDC37 interaction, but instead directly impacts the interaction between HSP90β and HER2 (Fig. 3D). Conversely, treatment with the specific ATM inhibitor, KU-55933, impinged on HSP90-CDC37 interaction (Fig. 3D), suggesting that ATM may affect HSP90 functionality through a more complex signaling only partially dependent on T297 phosphorylation.

2.4. HSP90β phosphorylation on T297 promotes HER2 dependent in vitro tumorigenicity

It has been previously reported that cancer cells may become addicted to HER2 aberrant expression and that in these contexts the downregulation of HER2 expression or the targeting of HER2 signaling may result in reduced cell viability and tumorigenicity [49,50]. Consistently with the key role of HSP90 as guardian of HER2 stability, HSP90 has been identified as a valuable target to counteract HER2 tumorigenicity (reviewed in [51]). Indeed, genetic inhibition of HSP90β by specific shRNA, triggers as expected the strong downregulation of HER2 and dramatically arrests SKBR3 cells as shown by p21 accumulation (Supplementary Fig. S1E). To investigate whether HSP90β phosphorylation on T297 may impinge on HER2 expression and signaling, SKBR3 cells were transiently transfected with either HA-HSP90β WT or HA-HSP90β T297A. Again, the overexpression of HA-HSP90β T297A triggers the reduction of HER2 expression levels and more importantly impinges on its downstream signaling, particularly affecting AKT activation (Fig. 4A and Supplementary Fig. S2A). To further investigate the significance of T297 phosphorylation in the control of HER2-dependent cell viability, HA-HSP90β WT, HA-HSP90β T297A and HA-HSP90β T297D, were transiently transfected in both SKBR3 cells that endogenously overexpress HER2 and in the MCF7-HER2 cells stably transfected with HER2 (Supplementary Fig. S2B). MTS assays after 72 h of transfections show that while the overexpression of either HSP90β WT or HSP90β T297D did not affect cell viability, the overexpression of HSP90β T297A mutant severely impinged on MCF7-HER2 as well as on SKBR3 cellular viability (Fig. 4B). The same construct had no effect on MCF7 cells consistently with the notion that these cells are not addicted to HER2 and indeed do not depend on HER2 expression levels (Fig. 4B). To further clarify whether HSP90β phosphorylation on T297 selectively promotes HER2-dependent tumorigenicity, we transformed MCF10A cells, an established normal human mammary gland epithelial cellular system, with a constitutively active form of HER2 (NeuV664E, named NeuT) (Supplementary Fig. S2C). It is well-known that the overexpression of NeuT can trigger neoplastic transformation in normal mammary epithelial cells, such as MCF10A [52] and therefore enhances the stem-like property of these cells measured as their ability of MCF10A to grow in 3D as mammospheres [53]. As expected, we confirmed that MCF10A-NeuT cells exhibit increased sphere-forming ability and larger sphere size compared to cells infected with the control retrovirus (pBABE) (Fig. 4C, D, E). More interestingly, transfection of MCF10A-NeuT cells with a construct expressing HSP90β T297A inhibits both the sphere-forming ability and size of MCF10A-NeuT-derived mammospheres. Overall, these data suggest that HSP90β T297A may act as a dominant negative and therefore that phosphorylation at T297 may sustain HER2 expression, stability and functionality.

3. Discussion

The Heat Shock Protein 90 (HSP90) chaperone is a master controller of protein folding and proteostasis under both physiological and stress conditions. HSP90 has several hundred client proteins that play central roles in different signaling cascades and it is therefore involved in many cellular processes including cell proliferation, survival, neoplastic transformation, DNA repair, neurodegeneration and immune response [54]. Its key role in cancer is supported by the evidence that HSP90 expression is often upregulated during cancer development and its activity is crucial to stabilize many oncogenic client proteins [55]. In this context, the development of HSP90 inhibitors has been pursued by several laboratories to exploit them as new therapeutics. Evidence exists that these inhibitors could also be used in combination with chemotherapy, molecular targeted agents, or immunotherapy treatment approaches [56]. In addition, several studies aimed to uncover the molecular mechanisms that can modulate HSP90 functionality highlighted post-translational modifications (PTMs) including phosphorylation, as key regulators of HSP90 activity and ability to bind to co-chaperones as well as specific client proteins [57].

We previously demonstrated that HER2 activity can drive the activation of ATM, that in turn enhances the interaction between HSP90 and HER2 [39]. Here we identify a novel interplay between ATM kinase, HSP90 and HER2 tyrosine kinase receptor. We report that in HER2 positive tumors, ATM kinase can drive HSP90β phosphorylation on Threonine 297 (T297) which in turn enhances HSP90β ability to bind and stabilize HER2, promoting its oncogenic potential (Fig. 5). Computational investigation of the impact of the PTM on the functional dynamics of HSP90 shows that phosphorylation on T297 introduces significant changes in the internal rigidity patterns of HSP90β that are already detectable on the μs timescale. Importantly, what begins as a local disruption and reassembly of interactions leads to far-reaching modulations in motion, encompassing regions that determine biological function, including the client-binding lumen. While at the simulated timescales we do not directly observe any appreciable large-scale remodeling of the lumen in pT297 compared to HSP90β WT , based on our data, we propose a model whereby phosphorylation induces a general increase in inter-residue coordination, resulting in the selection of dynamic states preorganized for client-recruiting. In other words, higher collective fluctuations induced by phosphorylation underpin more favorable adaptation and binding to HER2. This would in turn translate in an enhanced ability of the chaperone to protect HER2 from unfolding and degradation, thus leading to increase its levels. Importantly, immunoprecipitation experiments demonstrate that the unphosphorylatable mutant HSP90β T297A, generated by point mutagenesis, is significantly impaired in its ability to interact and stabilize HER2 as its overexpression triggers HER2 ubiquitination and degradation. Consistently, we could show that the ectopic expression of HSP90β T297A dramatically impinges on HER2 ability to drive and sustain neoplastic transformation in mammary epithelial cellular models. As a specific kinase-targeting co-chaperone, CDC37 selectively recognizes and combines unfolded kinase clients before binding open-state HSP90. When HSP90-CDC37-kinase complexes are established, HSP90 integrates ATP and adopts a closed state to accomplish a regular kinase folding process. Therefore, the HSP90-CDC37 complex synergistically acts as a facilitator of oncogenesis to help the correct folding of a wide range of overexpressed or mutated oncogenic proteins, accelerating tumorigenic influence [49]. Compound that binds HSP90 N-terminus disrupt its interaction with CDC37 [48]. Interestingly, we found that expression of unphosphorylatable mutant HSP90β T297A does not

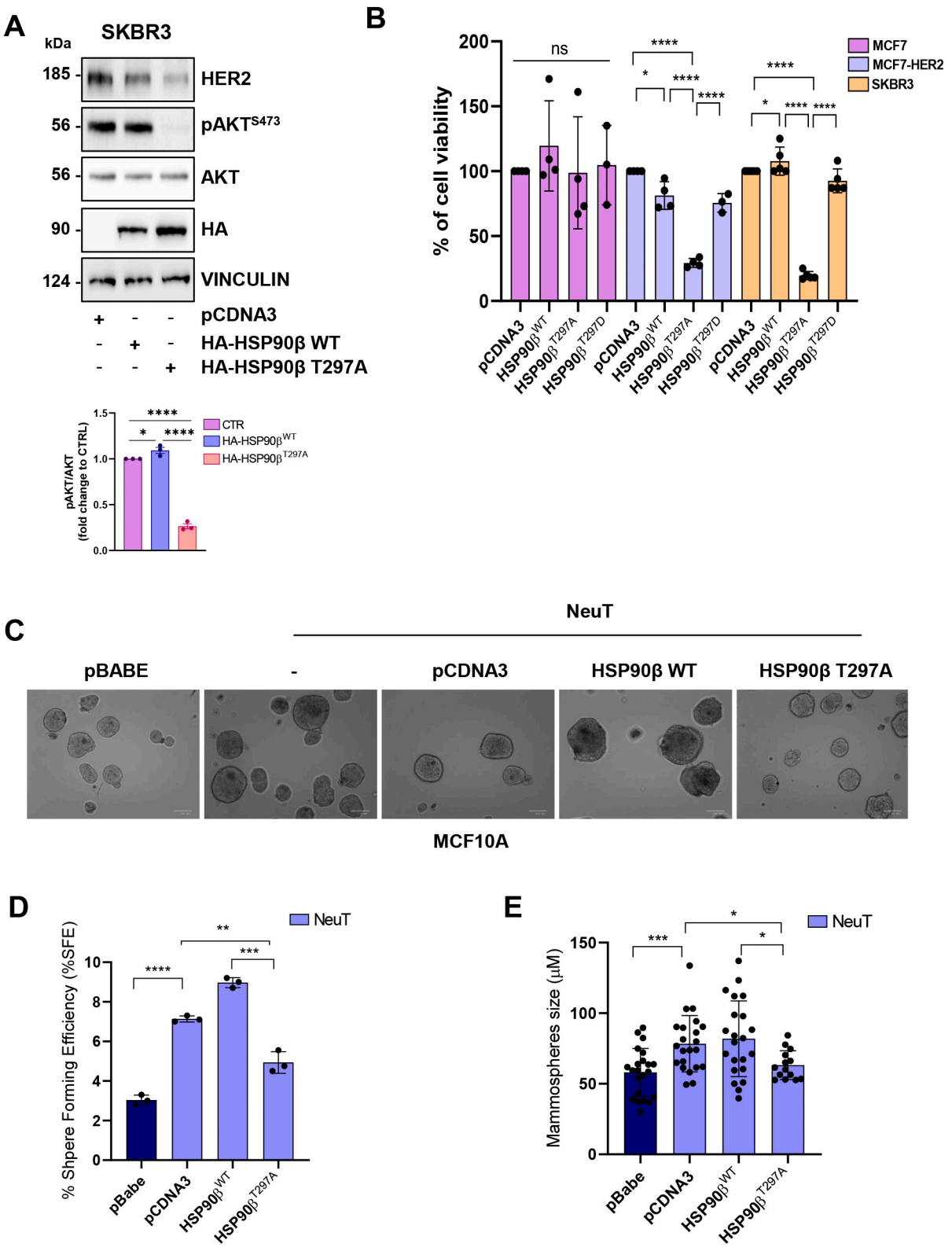

Fig. 4. HSP90β phosphorylation on T297 promotes HER2 tumorigenicity. (A) Representative Western blot showing pAKT^{S473}, AKT and HER2 protein levels in SKBR3 (HER2+++) cells transfected as indicated. On the bottom, quantification of pAKT^{S473} normalized on AKT total levels. (B) MTS assays performed after 48 h post transfection with the indicated constructs, HSP90β WT (HSP90^{WT}), HSP90β T297A (HSP90^{T297A}) and HSP90β T297D (HSP90^{T297D}), in MCF7, MCF7-HER2, SKBR3 cell lines. To determine if there are statistically significant differences in cell viability between multiple experimental groups we performed ANOVA one-way statistical test: ***, $P \leq 0.01$ MCF7 HER2 HSP90^{T297A} *vs* CTR; ****, $P \leq 0.001$ SKBR3 HSP90^{T297A} *vs* CTR. (C) Representative images of mammospheres formed from MCF10A cell lines transfected as indicated. (D, E) Histograms represent the sphere formation efficiency (SFE, at least 230 mammospheres per condition; $n = 3$) (D) and mammospheres size for the three cell lines (at least 50 mammospheres per condition; n = 3) (E).

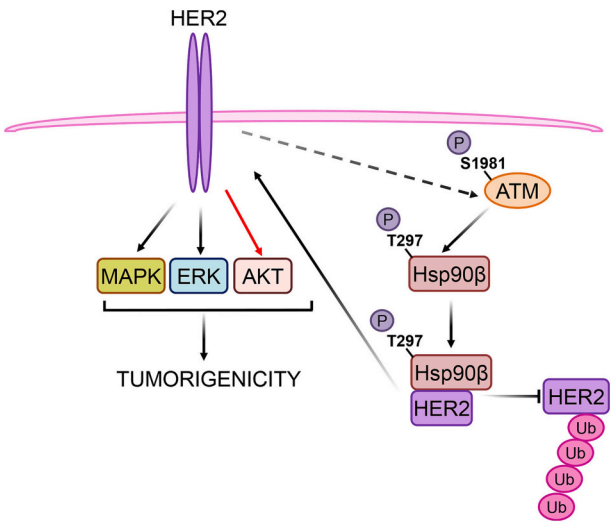

Fig. 5. Schematic model showing the interplay between HER2-ATM-HSP90β HER2 activity can drive ATM kinase activation which in turn triggers HSP90β phosphorylation on Threonine 297 (T297). This event enhances HSP90β ability to bind and stabilize HER2, promoting its oncogenic potential.

impinge on HSP90-CDC37 interaction. Conversely, ATM kinase inhibition with KU-55933 affects this interaction. We can speculate that ATM activity impinges directly on HSP90-HER2 interaction *via* T297 phosphorylation and affects HSP90-CDC37 interaction independently of T297. Future experiments will further clarify this point.

The identification of ATM-dependent phosphorylation of HSP90β on T297 in HER2 positive cancer models suggest that ATM activity may ensure high levels of HER2 expression and may be predictive for cancer response to molecular targeted therapy approaches such as Trastuzumab treatment. Of note, HSP90β T297A impinges HER2 dependent AKT activation, supporting the idea that ATM-dependent phosphorylation of HSP90 drives HER2-dependent tumorigenicity [58]. It will be interesting to evaluate whether loss of ATM activity may be one of the mechanisms responsible for the decrease on HER2 expression and the development of resistance. Interestingly, T297 phosphorylation was at first identified in a wide phosphoproteomic study showing that ionizing radiation, that induces DNA damage and ATM kinase activation, can trigger the same phosphorylation [37]. This observation suggests that the activation of ATM by different stimuli, including DNA damage, may promote HER2 stability, therefore raising the question whether ionizing radiation or chemotherapeutic approaches that sustain ATM kinase activity may ultimately drive HER2 accumulation. In this regard, we can speculate that the activation of ATM kinase activity may stabilize and maintain HER2 protein levels giving the possibility to treat the cells with a targeted therapy like Trastuzumab, conversely ATM kinase inhibition may sensitize cells to DNA radio and chemotherapy.

In addition, ATM kinase has been reported to be activated also by oxidative stress, mitochondrial dysfunction, alterations in transcription, alternative splicing, and plays a role also in the control of metabolism and proteostasis [34]. Future studies will clarify whether these stimuli may also drive HSP90β phosphorylation on T297. Moreover, it will be interesting to clarify whether this phosphorylation may affect also HSP90's interaction with other client proteins or with co-chaperones. Of note, T297 is not conserved in HSP90α, the inducible isoform of HSP90. Interestingly, ATM kinase can also trigger the phosphorylation of HSP90α [39] on two N-terminal threonine residues (Threonine 5 and Threonine7) upon ionizing radiation treatment. These phosphorylations correlate with the kinetics of H2AX phosphorylation on S139 (γH2AX) and support the activation of the DNA damage response [42]. Moreover, evidence for a role of ATM as HSP90α client protein has been previously provided [59]. Interestingly ATM and DNAPK may both phosphorylate HSP90α on T5 and T7 [42]. Since ATM kinase inhibitor treatment did not abolish HSP90 phosphorylation, as shown in Fig. 1A/E, we could speculate that although we inhibit ATM activity, other DNA damage related kinases, such as ATR and DNAPK, may contribute to HSP90 phosphorylation. Overall, these data together with our results support a complex interplay between ATM and HSP90 proteins, suggesting that ATM expression/activity may impinge on the functionality of this master chaperone. In this regard, it will also be interesting to investigate whether a defect in HSP90 functionality may play a role also in Ataxia Telangiectasia, a rare recessive genetic disorder, associated with ATM loss of expression, characterized by cerebellar degeneration and higher predisposition to cancer development [34,36].

Overall, our study identifies ATM-dependent phosphorylation of HSP90β on T297 as a novel mechanism to modulate HSP90β functionality and HER2 protein stability (Fig. 5) and suggests that this interplay may play a role in the control of proteostasis as well as in cancer progression and therapy response.

4. Materials and methods

4.1. Antibodies and reagents

The following antibodies and reagents were used: anti-phospho-Ser1981-ATM (Cell Signaling, 1/500), anti-ATM (2C1; Santa Cruz Biotechnology 1/1000), anti-tubulin (Sigma 1/3000), Mouse anti-c-ErbB-2 protein monoclonal antibodies, clone TA-1 (anti-c-*neu*, Ab-5, Oncogene Science, for immunoprecipitations, 2 μg for 1 mg total extracts) and clone 3B5 (Ab-3, Oncogene Science, for western immunoblots, 1/1000), anti-Ub (*P4D1*, Santa Cruz Biotechnology, 1/500), anti-Hsp90 (F8, Santa Cruz Biotechnology, 1/10,000). Anti-phospho-Ser727-STAT3 (Cell signaling 1/1000), anti-STAT3 (Cell Signaling, 1/1000), anti-phopsho-Ser473-AKT (Cell Signaling, 1/1000), anti-AKT (Cell Signaling 1/1000), anti-phospho-ERK-T202-204 (Cell Signaling, 1/1000), anti-ERK (Cell Signaling, 1/1000), anti-phospho-T180/Y182-p38 (Cell Signaling, 1/1000), anti-p38 (Cell Signaling, 1/1000), anti-HA (Sigma,1/1000), anti-vinculin (Cell Signaling, 1/5000) CHX (Sigma), KU-55933 (Calbiochem) and Tanespimycin (17-AAG) (SIGMA No. S1141) are all commercially available.

4.2. DNA constructs

The shHSP90α and shHSP90β constructs were generated and they had the following sequence respectively: 5′-GAT CCC CGG AAA GAG CTG CAT ATT AAT TCA AGA GAT TAA TAT GCA GCT CTT TCC TTT TTA-3′; 5′-GAT CCC CGG CTG AGG CCG ACA AGA ATT TCA AGA GAA TTC TTG TCG GCC TCA GCC TTT TTA-3′. Control shRNA, siR5, has been described [60]. ATM was silenced by lentivirus-mediated expression of shRNA using pSIN18.cPPT.RNAi. p.EGFP.WPRE lentiviral vector. HSP90α and HSP90β were silenced by retroviral-mediated expression of shRNA using pRETRO-Super vector. HSP90β T297A and HSP90β T297D constructs were generated using the QuickChange site directed mutagenesis kit (Stratagene, La Jolla, CA, USA) using pcDNA3.1-Hygro-HA-HSP90β WT as template kindly provided by Prof. Antonio Rossi. Retroviral vectors pBabe, pBabe-H-RasV12 and pBabe-NeuT, constitutively active HER2 mutant (NeuV664E), for stable gene expression were kindly provided by M.J. Reginato [61].

4.3. Cell cultures and infections

All cell lines were grown at 37 °C in a CO_2 incubator (5%). Breast cancer cell lines MCF7, MCF7-HER2, SKBR3, were kindly provided by Dr. Oreste Segatto and Dr. Paola Nisticò and described in [39] Human breast MCF10A cells were grown in HuMEC Basal Serum-Free Medium supplemented with the HuMEC Supplement Kit, as described in reference [39]. Retroviruses and lentiviruses were produced in HEK293T cells by cotransfecting pRETRO-Super and pSIN18.cPPT.RNAi. p.EGFP.

WPRE lentiviral vector together with respective plasmids encoding for gag-pol and VSV-G proteins. Viral supernatants, collected 48 h post transfection, filtered through a 0.45-μm pore size filter, were added to the cells in the presence of 2 μg ml^{-1} polybrene. Forty-eight hours post infection with the retrovirus construct, cells were selected by 1 μg ml^{-1} of puromycin.

4.4. Immunoprecipitations and immunoblotting

Total cell extracts were prepared in lysis buffer (50 mM Tris-HCl, pH 7.5, 250 mM NaCl, 1% NP40, 5 mM EDTA, 5 mM EGTA, 1 mM phenylmethylsulfonyl fluoride, 25 mM NaF, 1 mM orthovanadate, 40 mM beta-glycerophosphate, 10 mg ml^{-1} TPCK, 5 mg ml^{-1} TLCK, 1 mg ml^{-1} leupeptin, 10 mg ml^{-1} soybean trypsin inhibitor and 1 mg ml^{-1} aprotinin) and clarified by centrifugation at 10,000 ×*g* for 10 min at 4 °C. For immunoblotting, 50 μg protein extract were separated by SDS–polyacrylamide gel electrophoresis, blotted onto nitrocellulose membrane and detected with specific antibodies.

HER2 receptor was immunoprecipitated from 2 mg of protein using anti-ErbB2 (c-Neu; Ab-5; Oncogene Science) and protein A-sepharose beads (Amersham). In the case of coimmunopreciptation experiments, cells were lysed in TMNS buffer (50 mM Tris-HCl, 150 mM NaCl, 20 mM $NaMoO_4$, 0.09% NP40, 1 mM phenylmethylsulfonyl fluoride, 25 mM NaF, 1 mM orthovanadate, 40 mM beta-glycerophosphate, 10 mg ml^{-1} TPCK, 5 mg ml^{-1} TLCK, 1 mg ml^{-1} leupeptin, 10 mg ml^{-1} soybean trypsin inhibitor and 1 mg ml^{-1} aprotinin), while for the ubiquitination assay cells were lysed with RIPA buffer (50 mM Tris pH 8, 150 mM NaCl, 1% NP40, 0.1% SDS, 0.5% NaDeoxycolate, plus 20 mM NEM (Sigma E1271), 1 mM phenylmethylsulfonyl fluoride, 25 mM NaF, 1 mM orthovanadate, 40 mM beta-glycerophosphate,10 mg ml^{-1} TPCK, 5 mg ml^{-1} TLCK, 1 mg ml^{-1} leupeptin, 10 mg ml^{-1} soybean trypsin inhibitor and 1 mg ml^{-1} aprotinin).

4.5. In vitro ATM kinase assay

HEK293T cells were harvested and lysed in lysis buffer for 10 min on ice; then 1 mg of the lysate was precleared with protein A-coupled sepharose beads for 1 h and this was followed by incubation with anti-ATM antibodies overnight and addition of protein A beads for 1 h. Beads were centrifuged and washed three times with lysis buffer and once with kinase buffer (50 mM HEPES pH 7.5, 50 mM KCl; 5 mM MgCl2; 1 mM DTT and 10% glycerol) for 5 min for wash. Immunoprecipitated ATM was incubated with 1 μg of recombinant purified human HSP90β (ENZO ADI-SPP-777 - HSP90beta recombinant protein) substrate in kinase buffer. Then it was added of 10 ng of DNA-1 kb ladder (PROMEGA) to mimic DNA damage and ATM activation and 1 mM ATP. Kinase assay was allowed by incubation at 30 °C for 90 min. The reaction was stopped by addition of sample buffer and boiling.

4.6. Mammosphere cultures

Single-cell suspensions of MCF10A (and derived; see below) cell lines were grown in ultralow attachment six-well plates (Corning) at a density of 4000 cells/ml as described in reference [62]. After 10 d, the diameters of mammospheres were measured in phase-contrast pictures (ZOE) using ImageJ software. Numbers of mammospheres (diameter > 50 μm) were counted, and the efficiency of mammosphere formation was evaluated (%SFE = number of mammospheres/number of plated cells * 100). The mammosphere pellet was collected by gentle centrifugation (300*g*, 5 min) for RNA and protein extraction.

4.7. MTS assay

Cell viability of MCF7, MCF7-HER2, SKBR3, and their derived mammospheres in the normal and treated conditions was measured by the MTS assay (Promega). In brief, cells were plated in adhesion conditions in TC-treated well at density 1000 cells/100 μL medium. After 48 h post transfection with lipofectamine 2000 (Life Technologies) the MTS solution (Promega) was added per well and incubated at 37 °C for 3 h. Finally, optical density (OD) was measured at 492 nm wavelength, and the survival rates were calculated.

4.8. Statistical analyses

Data were statistically analyzed using the InStat3 GraphPad 7 by (i) unpaired *t*-tests and ordinary one-way ANOVA multiple comparison tests for measurements of continuous variables; when samples were not normally distributed, the Mann–Whitney and Kruskal–Wallis tests, respectively, were used instead; (ii) chi-squared (and Fisher's exact) tests, in the contingency table analyses for measurements of categorical variables; and (iii) Spearman's (non-normally distributed samples) correlation for single-cell correlation analysis. The number of replicates and sample size are indicated in the corresponding figure legends. The criterion for statistical significance (*) was set at $P < 0.01$.

4.9. Models of the missing HSP90β loop (residues 220-273)

The initial structure from which we built all six models of phosphorylated and unphosphorylated HSP90β simulated here was a partly refined CryoEM structure of the chaperone in its Mg^{2+}- and ATP-bound closed state. This was kindly provided by Prof. David A. Agard UCSF. The structure featured both protomers already resolved from residues 2 to 219 and from residues 274 to 724—essentially leaving only Met1 and the unstructured loop preceding the middle domains to be modeled on both—and showed very good overlap with published CryoEM structures of closed HSP90β (*e.g.*, in PDB ID: 5fwk) [49], with a 0.848 Å root-mean-square deviation for backbone heavy atoms of all resolved parts.

To begin with, the *PyMOL* suite The PyMOL Molecular Graphics System, Version 3.0 Schrödinger, LLC was used to model Met1 at the *N*-terminus of both protomers. We then proceeded to obtain three distinct models of the unstructured loop from residues 220 to 273, again using *PyMOL* to 'glue' identical copies of each model onto protomer A and B. The first model, modAF, was directly taken from the AlphaFold database and was attached to the structure resolved by Agard using backbone heavy atoms of residues 216 and 281 on each protomer as the structurally most viable 'anchor points', meaning that residues 217–220 and 274–280 were discarded from Agard's structure in this case.

The remaining two loop models, which we label mod04 and mod22, were generated *via* the MODELLER package [43] on protomer A of our starting structure, and were the two best scoring models out of a set of 25: more details on the algorithm are provided as Supporting Information.

Duplicating mod04 and mod22 into protomer B of our starting structure thus led to a total of three starting models for WT HSP90β: the one with AF-generated loops (WT_{AF}), the one with mod04 (WT_{04}), and the one with mod22 (WT_{22}).

4.10. Structure preparation, phosphorylation, solvation

The three resulting HSP90β structures (Fig. 2) were first preprocessed with the *reduce* utility from *AmberTools* (v. 2021) [63], which added hydrogens and evaluated different Asn, Gln, and His sidechain orientations. Subsequently, protonation states of titratable residues were assessed using the *PropKa* package (v. 3.1), this operation was only carried out on WT_{AF}, and resulting protonation states were adopted across all remaining structures, including in the final phosphorylated models generated later (*vide infra*). No alterations were suggested except for extra protonation of His320 on both protomers; of the remaining histidines, 149, 458, and 676 in protomers A and B were modeled in their δ-tautomeric form, and the rest in their ε-tautomeric form. Finally, no disulfide bridges were introduced in any of the models.

The following passage entailed an initial preprocessing WT_{AF}, WT_{04},

and WT_{22} with the *tleap* utility [63] to adequately place —NH_3^+ and —COO^- terminal caps, and type atoms their atoms for simulation (forcefield details are provided in the next subsection). The three preprocessed systems then underwent a round of preminimization *in vacuo* using the *sander* utility [63] (details and script Supporting Information). This was merely to relax the few residues in each system that served as 'anchor points' to incorporate loop models into the starting structure. Thence, phosphorylated equivalents $pT297_{AF}$, $pT297_{04}$, and $pT297_{22}$ were generated from their corresponding preminimized WT system, using the "builder" module of the *PyMOL* suite The PyMOL Molecular Graphics System, Version 3.0 Schrödinger, LLC. to replace Thr297:Hγ with a $–PO_3^{2-}$ group.

Concluding the preparation was a second round of preprocessing with *tleap* on all six systems. First, crystallographic waters were added to the NTD and Middle-domain of both protomers in each system, based on their distribution in the available crystal structures of the isolated domains in question (PDB IDs: 6n8y, and 3pry, respectively). Each system was then solvated in a similarly sized regular truncated octahedral box of water molecules. The reference box size was that of the solvation box of the WT_{AF}/$pT297_{AF}$ couple, since AF-modeled loops were those extending the farthest away from the main HSP90β corpus; in turn, the WT_{AF} and $pT297_{AF}$ boxes were constructed so that edges fell no closer than 12.0 Å from any HSP90β atom. Finally, after solvation, a sufficient number of Na^+ countercations was randomly placed within each simulation box to restore the net charge to 0.

Coordinates and topologies of the six solvated systems issuing from these procedures—WT_{AF}, WT_{04}, WT_{22}, $pT297_{AF}$, $pT297_{04}$, and $pT297_{22}$—served as starting points for MD simulations, and are provided electronically as Supporting Information.

4.10.1. Forcefield details

Standard protein residues were simulated with the standard ff14SB forcefield [64], whereas pT297 in phosphorylated systems was treated with its modified variant phosaa14SB [65]. ATP molecules were treated as prescribed by Meagher et al. [66] Parameters for Mg^{2+} and Na^+ cations were those published by Allnér et al. [67] and by Joung and Cheatham [68] respectively. Water molecules were treated according to the TIP3P model.

4.10.2. MD simulation details

Molecular dynamics (MD) simulations of the three WT and three pT297 models of Hsp90β prepared above were conducted using the *Amber20* molecular simulation suite [69]. Each of the six systems was simulated in four independent replicates, each with a 1 μs long production stage, for a combined production time of 4 μs for each system, and a total production time of 24 μs overall. The production stage was run with the *pmemd.cuda* utility (benefitting from GPU-acceleration [70], in the *NpT* ensemble ($T = 300$ K, imposed by the Langevin thermostat [71] with a 5.0 ps^{-1} collision frequency; $p = 1$ atm, imposed by the Berendsen barostat with a 1.0 ps coupling constant).

Before production, each replica underwent (1) 300 minimization steps on certain non-water hydrogens; (2) 300 minimization steps on all atoms; and (3) a 2.069 ns MD preproduction run. The latter stage entailed solvent equilibration, heating, and system equilibration, with increasingly lax restraints.

Throughout all MD stages, we imposed a cutoff of 8 Å for the evaluation in direct space of Lennard-Jones and Coulomb interactions between nonbonded atom pairs. Beyond this, only Coulomb interactions are calculated, in reciprocal space, using the Particle Mesh Ewald approach. Full preproduction details and all input scripts are provided as Supporting Information.

4.10.3. DF analysis

In a world where allosteric phenomena tend to occur over longer timescales than those typically accessed by MD simulations [72,73], distance fluctuation (DF) analysis [73–75] can conveniently process an ordinary MD trajectory of a protein or protein complex, and easily detect groups of residues—even mutually distant ones—that move in a more coordinated fashion compared to others. Then, even if the MD simulation in question is not long enough to detect any major allostery-driven conformational changes, groups of particularly coordinated residues will represent the key hotspots that mediate allosteric processes; any alterations in coordination that may be introduced by a PTM like pT297 will, similarly, be indicative of a change in the allosteric behavior of the simulated species.

In this work, one distinct DF analysis was conducted on the combined MD metatrajectories (all 4 replicates) of WT_{AF}, WT_{04}, and WT_{22}; and another one was conducted on the combined MD metatrajectories of $pT297_{AF}$, $pT297_{04}$, and $pT297_{22}$. To perform the analysis, both metatrajectories had to be stripped of everything except Cα atoms. The code to do the analysis itself is available at https://github.com/colombolab/Distance-Fluctuation-DF-Analysis.

The key outcome of DF analysis for a protein (complex) with N residues is a $N \times N$ pairwise DF score matrix, in which the individual matrix element DF_{ij} represents the DF score between the i^{th} and j^{th} residues. A peculiarity of the DF analysis conducted for this work is that, as a further 'significance safety check', DF scores have additionally been filtered by the local flexibility parameter (*LF*). More specifically, pairwise DF_{ij} scores under this special filtration scheme are calculated as follows

$$\left.\begin{array}{ll} DF_{ij} = & \left\langle \left(d_{ij} - \langle d_{ij} \rangle\right)^2 \right\rangle \\ DF_{ij} = & 0 \end{array}\right\} \begin{array}{l} DF_{ij} \geq LF \\ DF_{ij} < LF \end{array}$$

where for nonzero DF_{ij} scores, values delimited by ⟨⟩ denote metatrajectory averages, and d_{ij} indicates the distance between Cα-Cα distance between residues *i* and *j*. For unfiltered scores, it is thus easy to see that residue pairs with the least average deviation from their average distance $\langle d_{ij} \rangle$ (*i.e.*, the least average fluctuation), will be the ones with the lowest DF score, but the highest degree of mutual allosteric coordination.

Instead, filtration by Local Fluctuation automatically sets DF_{ij} scores to 0, excluding associated residue pairs from the final analysis on the grounds of lesser statistical meaning, and resulting in empty regions in the final DF matrix. The *LF* value is the average (unfiltered) *DF* score of sequentially adjacent residue pairs. It is quantified as follows

$$LF = \frac{1}{N_{adj}} \sum_i \sum_{i<j<i+5} DF_{ij}$$

where N_{adj} is the number of residue pairs that are sequentially separated by 3 residues or less ($i < j < i + 5$). To give an idea, *LF* values calculated from our DF analysis are 0.66 Å for WT HSP90β and 0.65 Å for the pT297 variant.

Subtraction of the LF-filtered DF matrix derived from simulations of WT HSP90β from the LF-filtered DF matrix derived from simulations of the pT297 variant—as is done in Fig. 2B—can immediately reveal which areas lose mutual coordination upon phosphorylation (increase in LF-filtered DF scores) and which areas gain it (decrease in LF-filtered DF scores).

4.10.4. Lumen cross-section analysis

To calculate the lumen cross-section in each MD frame, we began by extracting the coordinates of four specific atoms (*cf.* Fig. 2C): Asn346:Cα from protomer A; its counterpart in protomer B; Ala610:C from protomer A; and its counterpart in protomer B. Coordinates of these atoms were extracted from MD metatrajectories of the WT and pT297 HSP90β variants frame-by-frame, using the *cpptraj* tool [76]. Thence, using an in-house script that is provided electronically, as Supporting Information, we calculated the plane that could best fit the four atoms (*i.e.*, the plane to which all four atoms are as close as possible). Projections of those atoms onto the plane form a distinct irregular quadrilateral in each MD frame: the lumen cross-section was taken to be the area of this

quadrilateral. The necessary mathematical operations to derive the cross-section in each MD frame are provided as Supporting Information.

Histograms of the distribution of the lumen cross-sections across simulations of WT and pT297 HSP90β were derived using the *Xmgrace* package.

Supplementary data to this article can be found online at https://doi.org/10.1016/j.bbamcr.2026.120110.

CRediT authorship contribution statement

Giulia Fianco: Methodology, Investigation. **Irene Taddei:** Methodology, Investigation, Data curation. **Veronica Oropallo:** Methodology, Investigation, Data curation. **Claudia Contadini:** Methodology, Investigation, Data curation. **Alessandra Ferri:** Methodology, Investigation, Data curation. **Laura Coculo:** Methodology, Investigation. **Stefano A. Serapian:** Methodology, Investigation, Data curation. **Giorgio Colombo:** Writing – review & editing, Writing – original draft, Methodology, Investigation, Data curation, Conceptualization. **Venturina Stagni:** Writing – review & editing, Writing – original draft, Supervision, Funding acquisition, Data curation, Conceptualization. **Daniela Barilà:** Writing – review & editing, Writing – original draft, Resources, Methodology, Investigation, Funding acquisition, Data curation, Conceptualization.

Declaration of competing interest

The authors declare that they have no known competing financial interests or personal relationships that could have appeared to influence the work reported in this paper.

Acknowledgements

This work has been supported by research grant from Associazione Italiana per la Ricerca sul Cancro AIRC-IG2021-n.26230 and by Italian Ministry of Health, RF-2016-02362022 to D.B.; National Recovery and Resilience Plan (NRRP), Mission 4, Component 2, Investment 1.1, Call No. 104 (2.2.2022) by the Italian Ministry of University and Research (MUR), funded by the European Union – NextGenerationEU – PRIN Project N. CUP B53D23015820006 (PRIN202224M22R, to V.S. and L. C.); C.C. has been supported by AIRC-IG2021-n.26230; I.T. is supported by a MUR fellowship to the PhD Program in Cellular and Molecular Biology, Department of Biology, University of Tor Vergata, G.F. has been supported by Italian Ministry of Health, RF-2016-02362022, V.O. has been supported by MIUR fellowship to the PhD Program in Cellular and Molecular Biology, Department of Biology, University of Tor Vergata and by PRIN. GC and SAS would like to thank 2AIRC (Grant IG2023-n.27139) for the kind financial support, and the *eos* interdepartmental High-Performance Computing facility of the University of Pavia. Thanks, are also due to Prof. David A. Agard (UCSF) for providing a refined CryoEM structure of WT Hsp90β. Work partially supported by Consiglio Nazionale delle Ricerche - CNR (project DSB.AD006.371-InvAt-FOE2022) to VS.

Data availability

No data was used for the research described in the article.

References

[1] M. Taipale, D.F. Jarosz, S. Lindquist, HSP90 at the hub of protein homeostasis: emerging mechanistic insights, Nat. Rev. Mol. Cell Biol. 11 (2010) 515–528.
[2] L.M. Silbermann, B. Vermeer, S. Schmid, K. Tych, The known unknowns of the Hsp90 chaperone, Elife 13 (2024).
[3] A.S. Sreedhar, E. Kalmar, P. Csermely, Y.F. Shen, Hsp90 isoforms: functions, expression and clinical importance, FEBS Lett. 562 (2004) 11–15.
[4] J.L. Johnson, Evolution and function of diverse Hsp90 homologs and cochaperone proteins, Biochim. Biophys. Acta 2012 (1823) 607–613.
[5] S. Maiti, D. Picard, Cytosolic Hsp90 isoform-specific functions and clinical significance, Biomolecules 12 (2022).
[6] T. Langer, S. Rosmus, H. Fasold, Intracellular localization of the 90 kDA heat shock protein (HSP90alpha) determined by expression of a EGFP-HSP90alpha-fusion protein in unstressed and heat stressed 3T3 cells, Cell Biol. Int. 27 (2003) 47–52.
[7] D. Picard, Heat-shock protein 90, a chaperone for folding and regulation, Cell. Mol. Life Sci. 59 (2002) 1640–1648.
[8] J.A. Heritz, S.J. Backe, M. Mollapour, Molecular chaperones: guardians of tumor suppressor stability and function, Oncotarget 15 (2024) 679–696.
[9] E.G. Mimnaugh, C. Chavany, L. Neckers, Polyubiquitination and proteasomal degradation of the p185c-erbB-2 receptor protein-tyrosine kinase induced by geldanamycin, J. Biol. Chem. 271 (1996) 22796–22801.
[10] S. Kumar, M. Basu, M.K. Ghosh, Chaperone-assisted E3 ligase CHIP: a double agent in cancer, Genes Dis 9 (2022) 1521–1555.
[11] T.S. Reynolds, B.S.J. Blagg, Extracellular heat shock protein 90 alpha (eHsp90alpha)'s role in cancer progression and the development of therapeutic strategies, Eur. J. Med. Chem. 277 (2024) 116736.
[12] Y. Li, J. Dong, J.J. Qin, Small molecule inhibitors targeting heat shock protein 90: an updated review, Eur. J. Med. Chem. 275 (2024) 116562.
[13] C. Prodromou, X. Aran-Guiu, J. Oberoi, L. Perna, J.P. Chapple, J. van der Spuy, HSP70-HSP90 chaperone networking in protein-misfolding disease, Subcell. Biochem. 101 (2023) 389–425.
[14] S. Rastogi, A. Joshi, N. Sato, S. Lee, M.J. Lee, J.B. Trepel, L. Neckers, An update on the status of HSP90 inhibitors in cancer clinical trials, Cell Stress Chaperones 29 (2024) 519–539.
[15] I. D'Annessa, S. Raniolo, V. Limongelli, D. Di Marino, G. Colombo, Ligand binding, unbinding, and allosteric effects: deciphering small-molecule modulation of HSP90, J Chem Theory Comput 15 (2019) 6368–6381.
[16] X.M. Yu, G. Shen, L. Neckers, H. Blake, J. Holzbeierlein, B. Cronk, B.S. Blagg, Hsp90 inhibitors identified from a library of novobiocin analogues, J. Am. Chem. Soc. 127 (2005) 12778–12779.
[17] E. Amatya, C. Subramanian, R. Long, K. McNamara, M.S. Cohen, B.S.J. Blagg, The investigation of Hsp90C-terminal inhibitors containing amide bioisosteres, ChemMedChem 19 (2024) e202400418.
[18] A. Paladino, M.R. Woodford, S.J. Backe, R.A. Sager, P. Kancherla, M.A. Daneshvar, V.Z. Chen, D. Bourboulia, E.F. Ahanin, C. Prodromou, G. Bergamaschi, A. Strada, M. Cretich, A. Gori, M. Veronesi, T. Bandiera, R. Vanna, G. Bratslavsky, S. A. Serapian, M. Mollapour, G. Colombo, Chemical perturbation of oncogenic protein folding: from the prediction of locally unstable structures to the design of disruptors of Hsp90-client interactions, Chemistry 26 (2020) 9459–9465.
[19] B. Birbo, E.E. Madu, C.O. Madu, A. Jain, Y. Lu, Role of HSP90 in cancer, Int. J. Mol. Sci. 22 (2021).
[20] Z.N. Li, Y. Luo, HSP90 inhibitors and cancer: prospects for use in targeted therapies (review), Oncol. Rep. 49 (2023).
[21] M. Galogre, D. Rodin, M. Pyatnitskiy, M. Mackelprang, I. Koman, A review of HER2 overexpression and somatic mutations in cancers, Crit. Rev. Oncol. Hematol. 186 (2023) 103997.
[22] C. Lohrisch, M. Piccart, HER2/neu as a predictive factor in breast cancer, Clin. Breast Cancer 2 (2001) 129–135, discussion 136-127.
[23] L. Wang, Y. Wang, Y. Li, L. Zhou, J. Du, J. Wang, S. Liu, Y. Cao, Y. Li, W. Yang, T. Zhu, Resistance mechanisms and prospects of trastuzumab, Front. Oncol. 14 (2024) 1389390.
[24] L. Neckers, E. Mimnaugh, T.W. Schulte, Hsp90 as an anti-cancer target, Drug Resist. Updat. 2 (1999) 165–172.
[25] H. Schwartz, B. Scroggins, A. Zuehlke, T. Kijima, K. Beebe, A. Mishra, L. Neckers, T. Prince, Combined HSP90 and kinase inhibitor therapy: insights from The Cancer Genome Atlas, Cell Stress Chaperones 20 (2015) 729–741.
[26] S.J. Backe, R.A. Sager, M.R. Woodford, A.M. Makedon, M. Mollapour, Post-translational modifications of Hsp90 and translating the chaperone code, J. Biol. Chem. 295 (2020) 11099–11117.
[27] M. Mollapour, S. Tsutsumi, Y.S. Kim, J. Trepel, L. Neckers, Casein kinase 2 phosphorylation of Hsp90 threonine 22 modulates chaperone function and drug sensitivity, Oncotarget 2 (2011) 407–417.
[28] M. Mollapour, S. Tsutsumi, L. Neckers, Hsp90 phosphorylation, Wee1 and the cell cycle, Cell Cycle 9 (2010) 2310–2316.
[29] M. Mollapour, L. Neckers, Post-translational modifications of Hsp90 and their contributions to chaperone regulation, Biochim. Biophys. Acta 2012 (1823) 648–655.
[30] M. Castelli, K. Bhattacharya, E. Abboud, S.A. Serapian, D. Picard, G. Colombo, Phosphorylation of the Hsp90 co-chaperone hop changes its conformational dynamics and biological function, J. Mol. Biol. 435 (2023) 167931.
[31] S.T. Kim, D.S. Lim, C.E. Canman, M.B. Kastan, Substrate specificities and identification of putative substrates of ATM kinase family members, J. Biol. Chem. 274 (1999) 37538–37543.
[32] S. Bhatti, S. Kozlov, A.A. Farooqi, A. Naqi, M. Lavin, K.K. Khanna, ATM protein kinase: the linchpin of cellular defenses to stress, Cell. Mol. Life Sci. 68 (2011) 2977–3006.
[33] Y. Shiloh, Y. Ziv, The ATM protein kinase: regulating the cellular response to genotoxic stress, and more, Nat. Rev. Mol. Cell Biol. 14 (2013) 197–210.
[34] J.H. Lee, T.T. Paull, Cellular functions of the protein kinase ATM and their relevance to human disease, Nat. Rev. Mol. Cell Biol. 22 (2021) 796–814.
[35] Y. Shiloh, ATM: expanding roles as a chief guardian of genome stability, Exp. Cell Res. 329 (2014) 154–161.
[36] V. Stagni, V. Oropallo, G. Fianco, M. Antonelli, I. Cina, D. Barila, Tug of war between survival and death: exploring ATM function in cancer, Int. J. Mol. Sci. 15 (2014) 5388–5409.

[37] S. Matsuoka, B.A. Ballif, A. Smogorzewska, E.R. McDonald 3rd, K.E. Hurov, J. Luo, C.E. Bakalarski, Z. Zhao, N. Solimini, Y. Lerenthal, Y. Shiloh, S.P. Gygi, S.J. Elledge, ATM and ATR substrate analysis reveals extensive protein networks responsive to DNA damage, Science 316 (2007) 1160–1166.
[38] M.P. Stokes, J. Rush, J. Macneill, J.M. Ren, K. Sprott, J. Nardone, V. Yang, S. A. Beausoleil, S.P. Gygi, M. Livingstone, H. Zhang, R.D. Polakiewicz, M.J. Comb, Profiling of UV-induced ATM/ATR signaling pathways, Proc. Natl. Acad. Sci. U. S. A. 104 (2007) 19855–19860.
[39] V. Stagni, I. Manni, V. Oropallo, M. Mottolese, A. Di Benedetto, G. Piaggio, R. Falcioni, D. Giaccari, S. Di Carlo, F. Sperati, M.T. Cencioni, D. Barila, ATM kinase sustains HER2 tumorigenicity in breast cancer, Nat. Commun. 6 (2015) 6886.
[40] T. O'Neill, A.J. Dwyer, Y. Ziv, D.W. Chan, S.P. Lees-Miller, R.H. Abraham, J.H. Lai, D. Hill, Y. Shiloh, L.C. Cantley, G.A. Rathbun, Utilization of oriented peptide libraries to identify substrate motifs selected by ATM, J. Biol. Chem. 275 (2000) 22719–22727.
[41] S. Santini, V. Stagni, R. Giambruno, G. Fianco, A. Di Benedetto, M. Mottolese, M. Pellegrini, D. Barilà, ATM kinase activity modulates ITCH E3-ubiquitin ligase activity, Oncogene 33 (2014) 1113–1123.
[42] A.L. Elaimy, A. Ahsan, K. Marsh, W.B. Pratt, D. Ray, T.S. Lawrence, M.K. Nyati, ATM is the primary kinase responsible for phosphorylation of Hsp90alpha after ionizing radiation, Oncotarget 7 (2016) 82450–82457.
[43] A. Fiser, A. Sali, Modeller: generation and refinement of homology-based protein structure models, Methods Enzymol. 374 (2003) 461–491.
[44] M. Varadi, D. Bertoni, P. Magana, U. Paramval, I. Pidruchna, M. Radhakrishnan, M. Tsenkov, S. Nair, M. Mirdita, J. Yeo, O. Kovalevskiy, K. Tunyasuvunakool, A. Laydon, A. Zidek, H. Tomlinson, D. Hariharan, J. Abrahamson, T. Green, J. Jumper, E. Birney, M. Steinegger, D. Hassabis, S. Velankar, AlphaFold Protein Structure Database in 2024: providing structure coverage for over 214 million protein sequences, Nucleic Acids Res. 52 (2024) D368–D375.
[45] G. Morra, R. Potestio, C. Micheletti, G. Colombo, Corresponding functional dynamics across the Hsp90 chaperone family: insights from a multiscale analysis of MD simulations, PLoS Comput. Biol. 8 (2012) e1002433.
[46] A. Rehn, E. Moroni, B.K. Zierer, F. Tippel, G. Morra, C. John, K. Richter, G. Colombo, J. Buchner, Allosteric regulation points control the conformational dynamics of the molecular chaperone Hsp90, J. Mol. Biol. 428 (2016) 4559–4571.
[47] M. Castelli, P. Yan, A. Rodina, C.S. Digwal, P. Panchal, G. Chiosis, E. Moroni, G. Colombo, How aberrant N-glycosylation can alter protein functionality and ligand binding: an atomistic view, Structure 31 (2023) 987–1004, e1008.
[48] L. Wang, L. Zhang, L. Li, J. Jiang, Z. Zheng, J. Shang, C. Wang, W. Chen, Q. Bao, X. Xu, Z. Jiang, J. Zhang, Q. You, Small-molecule inhibitor targeting the Hsp90-Cdc37 protein-protein interaction in colorectal cancer, Sci. Adv. 5 (2019) eaax2277.
[49] K.A. Verba, R.Y. Wang, A. Arakawa, Y. Liu, M. Shirouzu, S. Yokoyama, D.A. Agard, Atomic structure of Hsp90-Cdc37-Cdk4 reveals that Hsp90 traps and stabilizes an unfolded kinase, Science 352 (2016) 1542–1547.
[50] L.A. Carey, Breast cancer: HER2—a good addiction, Nat. Rev. Clin. Oncol. 9 (2012) 196–197.
[51] A. Citri, B.S. Kochupurakkal, Y. Yarden, The achilles heel of ErbB-2/HER2: regulation by the Hsp90 chaperone machine and potential for pharmacological intervention, Cell Cycle 3 (2004) 51–60.
[52] S. Li, J. Zhou, H. Wu, Q. Lu, Y. Tai, Q. Liu, C. Wang, Oncogenic transformation of normal breast epithelial cells co-cultured with cancer cells, Cell Cycle 17 (2018) 2027–2040.
[53] K.L. Harper, M.S. Sosa, D. Entenberg, H. Hosseini, J.F. Cheung, R. Nobre, A. Avivar-Valderas, C. Nagi, N. Girnius, R.J. Davis, E.F. Farias, J. Condeelis, C. A. Klein, J.A. Aguirre-Ghiso, Mechanism of early dissemination and metastasis in Her2(+) mammary cancer, Nature 540 (2016) 588–592.
[54] F.H. Schopf, M.M. Biebl, J. Buchner, The HSP90 chaperone machinery, Nat. Rev. Mol. Cell Biol. 18 (2017) 345–360.
[55] D. Mahalingam, R. Swords, J.S. Carew, S.T. Nawrocki, K. Bhalla, F.J. Giles, Targeting HSP90 for cancer therapy, Br. J. Cancer 100 (2009) 1523–1529.
[56] X. Liang, R. Chen, C. Wang, Y. Wang, J. Zhang, Targeting HSP90 for cancer therapy: current progress and emerging prospects, J. Med. Chem. 67 (2024) 15968–15995.
[57] T. Roychowdhury, S.W. McNutt, C. Pasala, H.T. Nguyen, D.T. Thornton, S. Sharma, L. Botticelli, C.S. Digwal, S. Joshi, N. Yang, P. Panchal, S. Chakrabarty, S. Bay, V. Markov, C. Kwong, J. Lisanti, S.Y. Chung, S.D. Ginsberg, P. Yan, E. De Stanchina, A. Corben, S. Modi, M.L. Alpaugh, G. Colombo, H. Erdjument-Bromage, T. A. Neubert, R.J. Chalkley, P.R. Baker, A.L. Burlingame, A. Rodina, G. Chiosis, F. Chu, Phosphorylation-driven epichaperome assembly is a regulator of cellular adaptability and proliferation, Nat. Commun. 15 (2024) 8912.
[58] L. Pan, J. Li, Q. Xu, Z. Gao, M. Yang, X. Wu, X. Li, HER2/PI3K/AKT pathway in HER2-positive breast cancer: a review, Medicine (Baltimore) 103 (2024) e38508.
[59] R. Pennisi, A. Antoccia, S. Leone, P. Ascenzi, A. di Masi, Hsp90alpha regulates ATM and NBN functions in sensing and repair of DNA double-strand breaks, FEBS J. 284 (2017) 2378–2395.
[60] M.P. Mongiardi, V. Stagni, M. Natoli, D. Giaccari, I. D'Agnano, M.L. Falchetti, D. Barilà, A. Levi, Oxygen sensing is impaired in ATM-defective cells, Cell Cycle 10 (2011) 4311–4320.
[61] K.K. Haenssen, S.A. Caldwell, K.S. Shahriari, S.R. Jackson, K.A. Whelan, A.J. Klein-Szanto, M.J. Reginato, ErbB2 requires integrin alpha5 for anoikis resistance via Src regulation of receptor activity in human mammary epithelial cells, J. Cell Sci. 123 (2010) 1373–1382.
[62] V. Stagni, A. Kaminari, Z. Sideratou, E. Sakellis, S.A. Vlahopoulos, D. Tsiourvas, Targeting breast cancer stem-like cells using chloroquine encapsulated by a triphenylphosphonium-functionalized hyperbranched polymer, Int. J. Pharm. 585 (2020) 119465.
[63] D.A. Case, H.M. Aktulga, K. Belfon, D.S. Cerutti, G.A. Cisneros, V.W.D. Cruzeiro, N. Forouzesh, T.J. Giese, A.W. Gotz, H. Gohlke, S. Izadi, K. Kasavajhala, M. C. Kaymak, E. King, T. Kurtzman, T.S. Lee, P. Li, J. Liu, T. Luchko, R. Luo, M. Manathunga, M.R. Machado, H.M. Nguyen, K.A. O'Hearn, A.V. Onufriev, F. Pan, S. Pantano, R. Qi, A. Rahnamoun, A. Risheh, S. Schott-Verdugo, A. Shajan, J. Swails, J. Wang, H. Wei, X. Wu, Y. Wu, S. Zhang, S. Zhao, Q. Zhu, T. E. Cheatham 3rd, D.R. Roe, A. Roitberg, C. Simmerling, D.M. York, M.C. Nagan, K. M. Merz Jr., AmberTools, J. Chem. Inf. Model. 63 (2023) 6183–6191.
[64] J.A. Maier, C. Martinez, K. Kasavajhala, L. Wickstrom, K.E. Hauser, C. Simmerling, ff14SB: improving the accuracy of protein side chain and backbone parameters from ff99SB, J Chem Theory Comput 11 (2015) 3696–3713.
[65] L.E. Raguette, A.E. Cuomo, K.A.A. Belfon, C. Tian, V. Hazoglou, G. Witek, S. M. Telehany, Q. Wu, C. Simmerling, phosaa14SB and phosaa19SB: updated Amber force field parameters for phosphorylated amino acids, J. Chem. Theory Comput. 16 (2024).
[66] K.L. Meagher, L.T. Redman, H.A. Carlson, Development of polyphosphate parameters for use with the AMBER force field, J. Comput. Chem. 24 (2003) 1016–1025.
[67] O. Allner, L. Nilsson, A. Villa, Magnesium ion-water coordination and exchange in biomolecular simulations, J Chem Theory Comput 8 (2012) 1493–1502.
[68] I.S. Joung, T.E. Cheatham 3rd, Determination of alkali and halide monovalent ion parameters for use in explicitly solvated biomolecular simulations, J. Phys. Chem. B 112 (2008) 9020–9041.
[69] D.A. Case, T.E. Cheatham 3rd, T. Darden, H. Gohlke, R. Luo, K.M. Merz Jr., A. Onufriev, C. Simmerling, B. Wang, R.J. Woods, The Amber biomolecular simulation programs, J. Comput. Chem. 26 (2005) 1668–1688.
[70] R. Salomon-Ferrer, A.W. Gotz, D. Poole, S. Le Grand, R.C. Walker, Routine microsecond molecular dynamics simulations with AMBER on GPUs. 2. Explicit solvent particle mesh ewald, J Chem Theory Comput 9 (2013) 3878–3888.
[71] R.J. Loncharich, B.R. Brooks, R.W. Pastor, Langevin dynamics of peptides: the frictional dependence of isomerization rates of N-acetylalanyl-N′-methylamide, Biopolymers 32 (1992) 523–535.
[72] G. Colombo, Computing allostery: from the understanding of biomolecular regulation and the discovery of cryptic sites to molecular design, Curr. Opin. Struct. Biol. 83 (2023) 102702.
[73] M. Castelli, F. Marchetti, S. Osuna, F.O. AS, A.J. Mulholland, S.A. Serapian, G. Colombo, Decrypting allostery in membrane-bound K-Ras4B using complementary in silico approaches based on unbiased molecular dynamics simulations, J. Am. Chem. Soc. 146 (2024) 901–919.
[74] E. Moroni, D.A. Agard, G. Colombo, The structural asymmetry of mitochondrial Hsp90 (Trap1) determines fine tuning of functional dynamics, J Chem Theory Comput 14 (2018) 1033–1044.
[75] M. Castelli, A. Magni, G. Bonollo, S. Pavoni, F. Frigerio, A.S.F. Oliveira, F. Cinquini, S.A. Serapian, G. Colombo, Molecular mechanisms of chaperone-directed protein folding: insights from atomistic simulations, Protein Sci. 33 (2023) e4880.
[76] D.R. Roe, T.E. Cheatham 3rd, PTRAJ and CPPTRAJ: software for processing and analysis of molecular dynamics trajectory data, J. Chem. Theory Comput. 9 (2013) 3084–3095.